Inorg. Chem. **2007**, *46*, 7731–7741

Crystallographic and Vibrational Spectroscopic Studies of Octakis(DMSO)lanthanoid(III) Iodides

Alireza Abbasi,[†,‡] Emiliana Damian Risberg,[†] Lars Eriksson,[†] János Mink,[||] Ingmar Persson,[*,£] Magnus Sandström,[*,†] Yurii V. Sidorov,[†,§] Mikhail Yu. Skripkin,[†,§] and Ann-Sofi Ullström[£]

Department of Physical, Inorganic and Structural Chemistry, Stockholm University, SE-106 91 Stockholm, Sweden, School of Chemistry, University College of Science, University of Tehran, P.O. Box 14155-6455, Tehran, Iran, Department of Chemistry, St. Petersburg State University, Universitetsky pr., 26, 198504 St. Petersburg, Russia, Department of Chemistry, Swedish University of Agricultural Sciences, P.O. Box 7015, SE-750 07 Uppsala, Sweden, and Department of Molecular Spectroscopy, Chemical Research Center of the Hungarian Academy of Sciences, P.O. Box 77, H-1525 Budapest, Hungary, Faculty of Information Technology, Research Institute of Chemical and Process Engineering, Pannon University, Veszprém, P.O. Box 158, Hungary

Received April 5, 2007

The octakis(DMSO) (DMSO = dimethylsulfoxide) neodymium(III), samarium(III), gadolinium(III), dysprosium(III), erbium(III), and lutetium(III) iodides crystallize in the monoclinic space group $P2_1/n$ (No. 14) with $Z = 4$, while the octakis(DMSO) iodides of the larger lanthanum(III), cerium(III), and praseodymium(III) ions crystallize in the orthorhombic space group *Pbca* (No. 61), $Z = 8$. In all $[Ln(OS(Me_2)_8]I_3$ compounds the lanthanoid(III) ions coordinate eight DMSO oxygen atoms in a distorted square antiprism. Up to three of the DMSO ligands were found to be disordered and were described by two alternative configurations related by a twist around the metal–oxygen (Ln–O) bond. To resolve the atomic positions and achieve reliable Ln–O bond distances, complete semirigid DMSO molecules with restrained geometry and partial occupancy were refined for the alternative sites. This disorder model was also applied on previously collected data for the monoclinic octakis(DMSO)yttrium(III) iodide. At ambient temperature, the eight Ln–O bond distances are distributed over a range of about 0.1 Å. The average value increases from Ln–O 2.30, 2.34, 2.34, 2.36, 2.38, 2.40 to 2.43 Å (Ln = Lu, Er, Y, Dy, Gd, Sm, and Nd) for the monoclinic $[Ln(OSMe_2)_8]I_3$ structures, and from 2.44, 2.47 to 2.49 Å (Ln = Pr, Ce, and La) for the orthorhombic structures, respectively. The average of the La–O and Nd–O bond distances remained unchanged at 100 K, 2.49 and 2.43 Å, respectively. Despite longer bond distances and larger Ln–O–S angles, the cell volumes are smaller for the orthorhombic structures (Ln = Pr, Ce, and La) than for the monoclinic structure with Ln = Nd, showing a more efficient packing arrangement. Raman and IR absorption spectra for the $[Ln(OS(CH_3)_2)_8]I_3$ (Ln = La, Ce, Pr, Nd, Gd, Tb, Dy, Er, Lu, and Y) compounds, also deuterated for La and Y, have been recorded and analyzed by means of normal coordinate methods. The force constants for the Ln–O and S–O stretching modes in the complexes increase with decreasing Ln–O bond distance and show increasing polarization of the bonds for the smaller and heavier lanthanoid(III) ions.

Introduction

Dimethylsulfoxide (DMSO) is an efficient aprotic solvent for electrolytes. The high permittivity ($\epsilon = 46.6$), strong electron-pair donor ability ($D_S = 27.5$; compared to 17 for water), and high molecular dipole moment ($\mu = 3.96$ D) provide the capability to solvate both soft and hard metal ions well.[1,2] Crystalline DMSO solvates of metal ions are useful as water-free precursors in inorganic syntheses.[3−5] For

* To whom correspondence should be addressed. E-mail: magnuss@struc.su.se (M.S.).
† Stockholm University.
‡ University of Tehran.
§ St. Petersburg State University.
£ Swedish University of Agricultural Sciences.
|| Chemical Research Center of the Hungarian Academy of Sciences; Pannon University.

(1) Martin, D.; Hauthal, H. G. *Dimethyl Sulfoxide*; Van Nostrand Reinhold: Wokingham, UK, 1975.
(2) Sandström, M.; Persson, I.; Persson, P. *Acta Chem. Scand.* **1990**, *44*, 653−675.
(3) Alessio, E. *Chem. Rev.* **2004**, *104*, 4203−4242.

10.1021/ic7006588 CCC: $37.00
Published on Web 08/24/2007

the fully DMSO-solvated lanthanoid(III) ions, the few crystal structures reported all show discrete oxygen-coordinated octakis(DMSO)lanthanoid(III) complexes, e.g., in bromide and perchlorate salts.[6−13] In the solvated lanthanoid(III) nitrates, the nitrate ion acts as a bidentate ligand with the lighter lanthanoid(III) ions coordinating four and the heavier three DMSO molecules,[14,15] consistent with the decreasing ionic radii for octa-coordination in the series of the highly charged lanthanoid(III) ions,[16] from 1.16 Å for lanthanum(III) to 0.98 Å for lutetium(III).[13,17,18]

The mode of metal ion coordination of DMSO is often characterized by means of crystallography and IR absorption spectroscopy.[3−5] In the current study, we have determined the Ln−O bond distances and coordination geometry by solving the crystal structures of several octakis(DMSO)-lanthanoid(III) iodides, $[Ln(OSMe_2)_8]I_3$, Ln = La, Ce, Pr, Nd, Sm, Gd, Dy, Er, and Lu. The iodide salts were chosen because the "soft" iodide ions, which do not bind to the "hard" lanthanoid(III) ions, interact only weakly with the DMSO ligands, and provide, in contrast to the perchlorate or trifluoromethanesulfonate anions, no crystallographic orientational disorder or additional vibrational bands.

The IR band dominated by S−O stretching for a DMSO monomer occurs in liquid DMSO at 1070 cm^{-1}.[19] A downshift of the band signifies solvation via the sulfoxide oxygen atom, as for the lanthanoid(III) ions.[4,20−24] The frequency of the dominating IR absorption band, assigned as S−O stretching, has been reported to shift in a region from about 907 cm^{-1} for O-bonded up to 1154 cm^{-1} for S-bonded DMSO ligands and has been used for correlations with S−O bond lengths.[4] However, overlapping bands give rise to assignment problems in this spectral region, and the complex nature of the mixed vibrational mode, including the interaction between the Ln−O and S−O bonds, with partial double bond character of the latter, sometimes obscures such correlations.

We have previously reported comprehensive vibrational and sulfur K-edge X-ray absorption near-edge structure (XANES) spectroscopic studies of the hexa-solvated trivalent Group 13 ions, aluminum(III), gallium(III), indium(III), and thallium(III).[25,26] The metal ion−oxygen bonding and the effects on the DMSO ligands were correlated to the ionic size. Significant changes were observed in the XANES spectra, especially pronounced for the soft thallium(III) ion. In the current work, mid-IR, far-IR, and Raman spectra were collected for the octa-solvated lanthanoid(III) complexes and analyzed with normal coordinate methods using the geometry from the crystal structures. For the lanthanum(III) and yttrium(III) iodides, the deuterated DMSO complexes (for previously obtained data)[27] were also included.

Experimental Section

Preparation of Crystalline Octakis(DMSO)lanthanum(III) (1), Cerium(III) (2), Praseodymium(III) (3), Neodymium(III) (4), Samarium(III) (5), Gadolinium(III) (6), Terbium(III), Dysprosium(III) (7), Erbium(III) (8), Lutetium(III) (9), and Yttrium Iodides. DMSO (Merck) was distilled over calcium hydride (Fluka) under vacuum prior to use. Deuterated DMSO, DMSO-d_6 (Merck), of analytical grade was used without further purification. The anhydrous metal iodides (Aldrich, 99.99%) were dissolved in excess of DMSO under inert atmosphere in exothermic reactions, and the solutions were slowly cooled to room temperature. Crystals of $[M(OSMe_2)_8]I_3$, M = La, Ce, Pr, Nd, Sm, Gd, Tb, Dy, Er, Lu, and Y, and $[M(OSMe_2\text{-}d_6)_8]I_3$, M = La and Y, solvates were obtained after partly evaporating the solvent at reduced pressure.

Crystallography. Data collections were performed using Mo Kα X-ray radiation at ambient temperature on single crystals enclosed in thin-walled glass capillaries. For **3**, **6**, **8**, and **9**, a Bruker SMART X-ray diffractometer equipped with a CCD detector (crystal-to-detector distance 5.00 cm) was used, for **5** and **7**, a STOE imaging plate diffractometer, and for **1**, **1*** (100 K), **2, 4**, and **4*** (100 K), an Oxford Instruments Xcalibur diffractometer. The Bruker, STOE IPDS, and CrysAlis program packages, respectively, were used for indexing and integrating the crystal reflections. For data reduction and empirical absorption corrections, the Bruker program packages SAINT and SADABS were used,[28] except for the absorption corrections of STOE and X-calibur data, which were performed with the programs X-RED and X-Shape, using symmetry-equivalent reflections to model crystal shape and size.[29] The structures were solved by direct methods and refined using full-matrix least-squares on F^2 by means of SHELXTL and SHELXL97.[30]

(4) Calligaris, M. *Coord. Chem. Rev.* **2004**, *248*, 351−375.
(5) Calligaris, M.; Carugo, O. *Coord. Chem. Rev.* **1996**, *153*, 83−154.
(6) Chan, E. J.; Cox, B. G.; Harrowfield, J. M.; Ogden, M. I.; Skelton, B. W.; White, A. H. *Inorg. Chim. Acta* **2004**, *357*, 2365−2373.
(7) Zhang, Q.-F.; Leung, W.-H.; Xin, X.-Q.; Fun, H.-K. *Inorg. Chem.* **2000**, *39*, 417−426.
(8) Cherkasova, T. G. *Zh. Neorg. Khim.* **1994**, *39*, 1316−1319.
(9) Cherkasova, T. G.; Anosova, Yu. V.; Shevchenko, T. M. *Zh. Neorg. Khim.* **2004**, *49*, 22−25.
(10) Plotnikova, T. E.; Grigor'ev, M. S.; Fedoseev, A. M.; Antipin, M. Yu. *Russ. J. Coord. Chem.*, **2004**, *30*, 60−67.
(11) Huang, Q.; Wu, X.; Lu, J. *Chem. Commun.* **1997**, 703−704.
(12) Klinga, M.; Cuesta, R.; Moreno, J. M.; Dominguez-Vera, J. M.; Colacio, E.; Kivekäs, R. *Acta Crystallogr.* **1998**, *C54*, 1275−1277.
(13) Sivapullaiah, P. V.; Soundararajan, S. *Current Sci.* **1975**, *44*, 374−376.
(14) Ramalingam, S. K.; Soundararajan, S. *Current Sci.* **1966**, *35*, 568; *J. Inorg. Nucl. Chem.* **1967**, *29*, 1763−1768.
(15) Bhandary, K. K.; Manohar, H. *Acta Crystallogr.* **1973**, *B29*, 1093−1098.
(16) Shannon, R. D. *Acta Crystallogr.* **1976**, *A32*, 751−767.
(17) Bünzli, J.-C. G.; Metabanzoulou, J.-P.; Froidevaux, P.; Jin, L. *Inorg. Chem.* **1990**, *29*, 3875−3881.
(18) Semenova, L. I.; Skelton, B. W.; White, A. H. *Aust. J. Chem.* **1996**, *49*, 997−1004.
(19) Skripkin, M. Yu.; Lindqvist-Reis, P.; Abbasi, A.; Mink, J.; Persson, I.; Sandström, M. *Dalton Trans.* **2004**, 4038−4049.
(20) *Gmelin Handbook of Inorganic Chemistry*, 8th ed.; Springer-Verlag: New York, 1986; Vol. D4, Chapter 1, pp 1−16.
(21) Cotton, F. A.; Francis, R.; Horrocks, W. D. *J. Phys. Chem.* **1960**, *64*, 1534−1536.
(22) Cotton, F. A.; Francis, R. *J. Am. Chem. Soc.* **1960**, *82*, 2986−2991.
(23) Horrocks, W. D.; Cotton, F. A. *Spectrochim. Acta* **1961**, *17*, 134−147.
(24) Johnson, B. F. G.; Walton, R. A. *Spectrochim. Acta* **1966**, *22*, 1853−1858.
(25) Molla-Abbassi, A.; Skripkin, M. Yu.; Kritikos, M.; Persson, I.; Mink, J.; Sandström, M. *Dalton Trans.* **2003**, 1746−1753.
(26) Damian, E.; Jalilehvand, F.; Abbasi, A.; Pettersson, L. G. M.; Sandström, M. *Phys. Scr.* **2005**, *T115*, 1077−1079.
(27) Lindqvist-Reis, P.; Näslund, J.; Persson, I.; Sandström, M. *J. Chem. Soc., Dalton Trans.* **2000**, 2703−2710.
(28) *SMART*, version 5.046; *SAINT*, 5.01 (integration software); *SADABS* (empirical absorption correction); Bruker Analytical X-ray Systems: Madison, WI, 1998.
(29) (a) *X-SHAPE*, version 1.02; STOE and Cie GmbH: Darmstadt, Germany, 1997. (b) *X-RED*, version 1.09; STOE and Cie GmbH: Darmstadt, Germany, 1997.

All the $[Ln(OS(CH_3)_2)_8]^{3+}$ complexes were found to have one or more disordered ligands. Since there are only minor variations in the internal geometry of those coordinated DMSO molecules (see below), restraints were imposed on the disordered ligands when refining the models of the crystal structures. The S−C and O−S bond distances and the intramolecular C···C and O···C distances were constrained to be equal (within 0.01 Å) to the corresponding values for a nondisordered DMSO ligand of the $[Ln(OS(CH_3)_2)_8]^{3+}$ complexes. In this way, semirigid molecular ligands in two different orientations (including 1 O, 1 S, and 2 C atoms for each) could be refined together with their site occupancy factors, while allowing a variation of ±0.01 Å in all distances. Close-lying oxygen positions could then be resolved for the disordered ligands, allowing reliable Ln−O bond distances to be obtained. All non-hydrogen atomic positions were refined anisotropically. The methyl hydrogen atoms were introduced at calculated positions with isotropic displacement parameters 1.5 times the corresponding displacement parameter of the methyl carbon atom. Selected crystallographic and experimental details are summarized in Table 1, and the Ln−O bond distances in Table 2.

Vibrational Spectra. Raman and IR. Raman spectra of the solid octakis(DMSO)lanthanoid(III) iodides were obtained using a Renishaw System 1000 spectrometer, equipped with a Leica DMLM microscope, a 25 mW diode laser (780 nm), and a Peltier-cooled CCD detector. The mid-IR (200−4000 cm^{-1}, resolution 4 cm^{-1}, 128 scans) absorption spectra of the solid compounds in CsI pellets were recorded in purged atmosphere using a Bio-Rad (Digilab) FTS 175 spectrometer. Far-IR spectra (range 50−700 cm^{-1}, resolution 2 cm^{-1}, 256 scans) were obtained from polyethylene pellets by means of a Bio-Rad (Digilab) FTS-40 spectrometer. All spectra were measured at ambient temperature.

Force Field Analysis. The 81 atoms of a $[Ln(OS(CH_3)_2)_8]^{3+}$ complex generate 237 fundamental vibrational modes. Detailed analysis of methyl C−H stretching, deformation, rocking, and torsional modes are of less importance in coordination studies than the ligand "skeletal" modes and the metal−ligand vibrations. Therefore, the calculations were simplified by introducing point masses for the methyl groups, which leaves 93 fundamental modes. Wilson's **GF** matrix method was used for the calculation of vibrational frequencies using a symmetrized valence force field. The initial set of the force constants was taken from our previous works.[19,25] As the first step, mono-ligand metal ion−DMSO entities were treated in C_s point group symmetry using averaged frequencies. Subsequently, all 33 non-hydrogen atoms were introduced for the $[Ln(OS(CH_3)_2)_8]^{3+}$ complexes in D_{4d} symmetry. The PC-based program package developed by J. Mink and L. Mink was used for the computational procedures.[31]

Results

Crystal Structures. The crystal structures of **1**−**3** were satisfactorily described in the orthorhombic space group *Pbca*, while the structures of **4**−**9** were characterized in $P2_1/n$ with the monoclinic angle close to 100° (Table 1). All crystal structures comprise discrete octakis(DMSO)lanthanoid(III) complexes and iodide ions. The lanthanoid(III) ions are surrounded by eight oxygen-bonded DMSO ligands with the oxygen atoms forming a distorted square antiprism. Disorder

Table 1. Crystallographic Data for $[Ln(OS(CH_3)_2)_8]I_3$ Compounds, Ln = La, Ce, Pr, Nd, Sm, Gd, Dy, Er, Lu (**1**−**9**), and La and Nd at 100 K (**1*** and **4***)

	1	**2**	**3**	**4**	**5**	**6**	**7**	**8**	**9**	**1***	**4***
formula	$C_{16}H_{48}S_8O_8I_3La$	$C_{16}H_{48}S_8O_8I_3Ce$	$C_{16}H_{48}S_8O_8I_3Pr$	$C_{16}H_{48}S_8O_8I_3Nd$	$C_{16}H_{48}S_8O_8I_3Sm$	$C_{16}H_{48}S_8O_8I_3Gd$	$C_{16}H_{48}S_8O_8I_3Dy$	$C_{16}H_{48}S_8O_8I_3Er$	$C_{16}H_{48}S_8O_8I_3Lu$	$C_{16}H_{48}S_8O_8I_3La$	$C_{16}H_{48}S_8O_8I_3Nd$
M_r	1144.63	1145.84	1146.63	1149.96	1156.07	1156.93	1168.22	1172.98	1180.69	1144.63	1149.96
cryst syst	orthorhombic	orthorhombic	orthorhombic	monoclinic	monoclinic	monoclinic	monoclinic	monoclinic	monoclinic	orthorhombic	monoclinic
space group	*Pbca* (No. 61)	*Pbca* (No. 61)	*Pbca* (No. 61)	$P2_1/n$ (No. 14)	$P2_1/n$ (No. 14)	$P2_1/n$ (No. 14)	$P2_1/n$ (No. 14)	$P2_1/n$ (No. 14)	$P2_1/n$ (No. 14)	*Pbca* (No. 61)	$P2_1/n$ (No. 14)
a/Å	19.3127(5)	19.2661(9)	19.015(9)	12.5319(6)	12.475(5)	12.4233(17)	12.3965(19)	12.3374(14)	12.257(3)	19.1406(10)	12.5379(2)
b/Å	19.5535(5)	19.4831(9)	19.363(9)	18.9941(10)	18.922(3)	18.929(3)	18.900(2)	18.853(2)	18.747(4)	19.3597(10)	18.6836(3)
c/Å	22.3396(6)	22.2279(11)	22.122(10)	18.1707(9)	18.131(6)	18.045(2)	18.036(3)	17.992(2)	17.933(4)	21.9325(10)	17.6653(3)
α, β, γ/°	90, 90, 90	90, 90, 90	90, 90, 90	90, 100.316, 90	90, 100.33, 90	90, 100.12, 90	90, 100.09, 90	90, 100.02, 90	90, 99.92, 90	90, 90, 90	90, 99.4694, 90
V/Å^3	8436.1(4)	8343.5(7)	8145(6)	4255.3(4)	4210(2)	4177.4(10)	4160.4(10)	4121.1(8)	4059.4(15)	8127.2(7)	4081.76(12)
T/K	295 ± 2	295 ± 2	295 ± 2	295 ± 2	295 ± 2	295 ± 2	295 ± 2	295 ± 2	295 ± 2	100 ± 2	100 ± 2
Z	8	8	8	4	4	4	4	4	4	8	4
D_{calcd}/g·cm^{-3}	1.802	1.824	1.870	1.795	1.824	1.849	1.865	1.891	1.932	1.871	1.871
μ(Mo Kα)/mm^{-1}	3.634	3.741	3.911	3.818	4.021	4.234	4.453	4.719	5.155	3.772	3.981
measured reflns	8259	39 232	42 685	8336	32 116	22 945	32 967	21 996	22 672	16 1947	13 669
unique reflns	8259 (R_{int} = 0.0698)	8162 (R_{int} = 0.0696)	8000 (R_{int} = 0.0874)	8336 (R_{int} = 0.045)	7817 (R_{int} = 0.0870)	8195 (R_{int} = 0.0369)	7795 (R_{int} = 0.0887)	8107 (R_{int} = 0.0442)	8188 (R_{int} = 0.0406)	18 691 (R_{int} = 0.0424)	13 669 (R_{int} = 0.0257)
observed reflns	4201	4218	4425	4321	5191	5780	5231	4778	5521	16 106	9987
final R1, wR2 [$I > 2\sigma(I)$][a]	0.0326, 0.0650	0.0501, 0.1010	0.0505, 0.1203	0.0437, 0.1075	0.0579, 0.1397	0.0406, 0.1024	0.0466, 0.1105	0.0639, 0.1783	0.0366, 0.0752	0.0514, 0.0835	0.0417, 0.1104
(all data)	0.0873, 0.0750	0.1409, 0.1245	0.1019, 0.1329	0.0762, 0.1111	0.0947, 0.1660	0.0667, 0.1095	0.0785, 0.1305	0.1074, 0.2070	0.0690, 0.0813	0.0674, 0.0882	0.0557, 0.1134

[a] *R* values are defined as $R1 = \sum||F_o| - |F_c||/\sum|F_o|$ and $wR2 = [\sum[w(F_o^2 - F_c^2)^2]/\sum[w(F_o^2)^2]]^{1/2}$.

(30) Sheldrick, G. M. *SHELXTL PLUS 1992*; University of Göttingen: Göttingen, Germany, 1992.

(31) Mink, J.; Mink, L. *Computer Program System for Vibrational Analyses of Polyatomic Molecules* (in Lahey-Fujitsu Fortran Win32); Stockholm, 2004.

Table 2. Ln−O Bond Distances in Å for $[Ln(OSMe_2)_8]I_3$, Ln = La, Ce, Pr, Nd, Sm, Gd, Dy, Er, Lu (**1**−**9**), and La and Nd at 100 K (**1*** and **4***)

	La (**1**)	Ce (**2**)	Pr (**3**)	Nd (**4**)	Sm (**5**)	Gd (**6**)	Dy (**7**)	Er (**8**)	Lu (**9**)	La (**1***)	Nd (**4***)
Ln−O1	2.517(3)	2.506(5)	2.418(5)	2.430(4)	2.419(5)	2.330(11)	2.379(4)	2.323(8)	2.286(6)	2.522(2)	2.434(3)
						2.373(13)		2.174(19)	2.14(2)		
Ln−O2	2.455(4)	2.492(5)	2.383(5)	2.474(8)	2.425(5)	2.383(4)	2.389(4)	2.359(5)	2.348(3)	2.456(2)	2.478(3)
				2.283(11)							2.417(12)
Ln−O3	2.450(4)	2.433(5)	2.476(5)	2.466(10)	2.376(12)	2.414(4)	2.391(5)	2.366(6)	2.321(3)	2.453(2)	2.376(3)
				2.309(9)	2.39(3)						
Ln−O4	2.528(3)	2.420(5)	2.389(5)	2.487(5)	2.336(14)	2.401(4)	2.390(5)	2.365(6)	2.262(4)	2.525(2)	2.457(3)
					2.399(19)						
Ln−O5	2.483(13)	2.416(5)	2.405(5)	2.361(11)	2.422(6)	2.405(4)	2.367(4)	2.298(6)	2.295(4)	2.498(10)	2.442(3)
	2.47(2)			2.447(14)						2.447(11)	
Ln−O6	2.526(4)	2.497(5)	2.519(14)	2.433(4)	2.417(6)	2.393(7)	2.356(6)	2.373(5)	2.337(3)	2.529(2)	2.453(3)
			2.428(16)			2.256(12)	2.159(19)				
Ln−O7	2.443(3)	2.453(5)	2.468(5)	2.456(4)	2.419(6)	2.398(4)	2.362(7)	2.344(16)	2.327(4)	2.4450(10)	2.371(4)
							2.185(14)	2.269(16)		2.488(11)	2.508(13)
Ln−O8	2.552(11)	2.48(2)	2.460(5)	2.460(4)	2.256(12)	2.348(6)	2.341(14)	2.346(6)	2.244(14)	2.542(5)	2.448(4)
	2.489(17)	2.530(14)			2.416(11)	2.37(2)	2.310(14)		2.303(11)	2.49(2)	2.228(10)

Table 3. Crystallographic Occupancy Factors in % (Estimated Standard Deviation ±1%) for Disordered DMSO Ligands in the $[Ln(OSMe_2)_8]I_3$ Compounds with Ln = La, Ce, Pr, Nd, Sm, Gd, Dy, Er, Lu (**1**−**9**) and Y at Ambient Temperature, and for La and Nd at 100 K (**1*** and **4***)

	occupancy factors for alternative DMSO sites (%)			mean Ln-O[a]	mean LnOS[a]	mean S−O[b]
Ln =	DMSO(A)	DMSO(B)	DMSO(C)	bond distance	bond angle	bond distance
La (**1***)	53/47	85/15	85/15	2.493	135.8	1.520
La (**1**)	61/39	60/40		2.490	138.3	1.504
Ce (**2**)	44/56			2.466	137.5	1.495
Pr (**3**)	54/46			2.435	136.7	1.491
Nd (**4***)	79/21	75/25	69/31	2.427	133.3	1.528
Nd (**4**)	63/37	52/48	52/48	2.433	136.9	1.493
Sm (**5**)	72/28	51/49	39/61	2.400	134.6	1.503
Gd (**6**)	51/49	68/32	81/19	2.382	133.1	1.504
Dy (**7**)	84/16	72/28	54/46	2.360	133.2	1.506
Er (**8**)	79/21	55/45		2.339	131.8	1.502
Lu (**9**)	83/17	41/59		2.304	131.4	1.506
Y	77/23	53/47	89/11	2.344	132.3	1.516

[a] The mean LnO bond lengths and LnOS angles were weigthed with the occupancy. [b] The mean S−O bond distances were calculated including only the ordered ligands.

was found to occur for all the solvates and was described by models with up to three disordered semirigid DMSO ligands (Figure 1). For each disordered ligand, two sites could be refined, mainly related by a twist around the Ln−O bond, with the site occupancy factors reported in Table 3. Previously, similar disorder has often been described simply by two partially occupied sulfur positions assuming inversion of the DMSO ligand. The overlapping non-resolved atomic positions result in high displacement parameters of the other ligand atoms,[32] while the disorder model employed in this study resolves all the atomic sites.

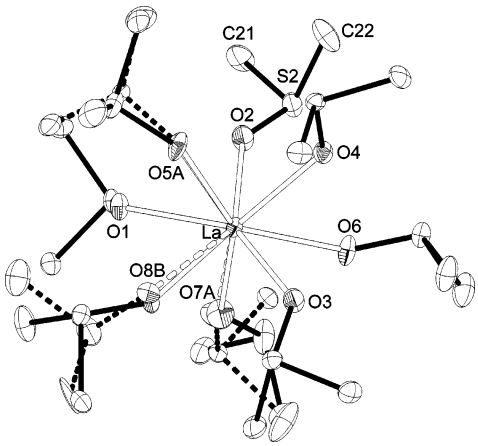

Figure 1. Octakis(DMSO)lanthanum(III) complex at 100 K in the $[La(OS(CH_3)_2)_8]I_3$ crystal structure with 40% probability ellipsoids.

The Ln−O bond distances listed in Table 2 show considerable distributions, often about 0.10 Å. The average values in Table 3 have been weighted with the occupancy factors for the disordered ligands. The current model with restrained DMSO geometries was also used for a recalculation of the previously studied octakis(DMSO)yttrium(III) iodide, which is isostructural to the monoclinic lanthanoid(III) iodide solvates.[27]

The mean Ln−O−S angle within the $[Ln(OSMe(CH_3)_2)_8]^{3+}$ complexes generally decreases when the lanthanoid(III) ions contract along the lanthanoid series, Figure 2. A decreasing MOS angle has previously been found to correspond to increasing M−O bond covalency.[25] For the monoclinic structures from Nd to Lu, the uniform decrease in unit cell volume corresponds to the decreasing size of the ions. However, the Ln = Pr, Ce, and La complexes have longer Ln−O bonds but smaller volumes (V/Z = 1018, 1043, 1055 Å^3, respectively) than that for the first monoclinic structure (Nd, 1064 Å^3). A plot of the unit cell volume per formula unit (V/Z) vs the mean Ln−O bond lengths illustrate the more efficient molecular packing in the orthorhombic symmetry (Figure 2). For all the lanthanoid(III) solvates, the surrounding iodide ions are in contact with the methyl hydrogen atoms of the DMSO ligands with the closest C(−H)···I$^-$ distances

(32) Harrowfield, J. M.; Richmond, W. R.; Skelton B. W.; White, A. H. *Eur. J. Inorg. Chem.* **2004**, 227−230.

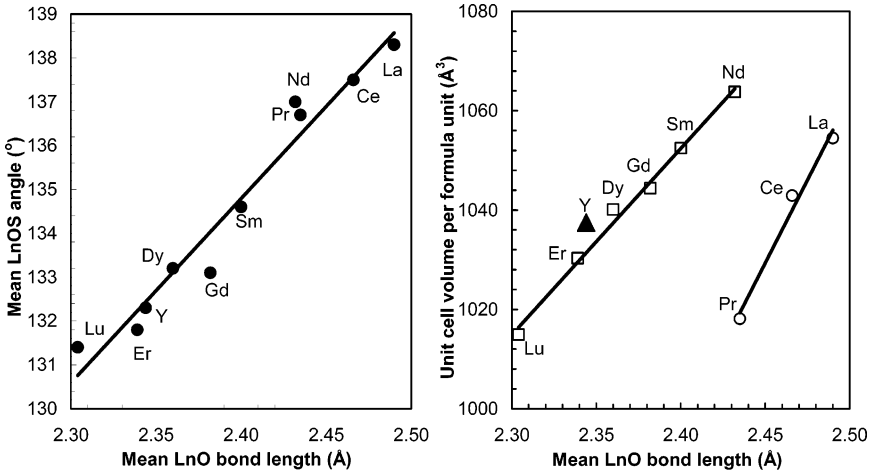

Figure 2. (left) Mean LnOS bond angle vs Ln−O bond length for the DMSO solvates $[Ln(OSMe_2)_8]I_3$ decreases fairly uniformly, while (right) the cell volume per formula unit (V/Z) displays a break at the phase transition with less-efficient packing for the smaller ions in the monoclinic structures.

at about 3.9 Å, slightly shorter than in the hexakis(DMSO)-scandium(III) iodide.[19]

Vibrational Spectra of $[Ln(OS(CH_3)_2)_8]^{3+}$ Complexes. The coordination of a DMSO molecule to a metal ion induces clearly visible changes in the vibrational spectra. These are frequency shifts of the $OSMe_2$ ligand modes due to changes in the internal bonding, splitting of degenerate IR- and Raman-active bands in the complex because of the vibrational interaction between the ligands, and the appearance of new metal−ligand vibrational modes. The D_{4d} point group symmetry is the highest possible for a $[Ln(OS(CH_3)_2)_8]^{3+}$ complex with point masses for the methyl groups (the description by means of 96 internal and 58 symmetry coordinates provided in Tables S1 and S2 includes three redundancies in the 8α and 8β angles). For idealized D_{4d} point group symmetry, out of the 93 normal vibrational modes belonging to the symmetry species $7A_1 + 4A_2 + 5B_1 + 7B_2 + 12E_1 + 12E_2 + 11E_3$, the A_1, E_2, and E_3 modes should be only Raman-active, while B_2 and E_1 should be only IR-active. The A_2 and B_1 modes are inactive in both the Raman and IR vibrational spectra. However, when assigning the bands in the experimental spectra, such definite selection rules must be exercised with caution. The IR and Raman bands of different symmetry species may appear coincident if the vibrational coupling is not strong enough for an observable separation. On the other hand, distortion of the complexes may allow modes forbidden in D_{4d} symmetry to appear as weak bands in the spectra.

The experimental IR and Raman fundamental frequencies for the $[Ln(OS(CH_3)_2)_8]^{3+}$ complexes are reported in Table 4. The assignment of the bands is based on the well-characterized spectrum of liquid DMSO,[19] aided by the results of the normal coordinate calculations. Spectra were also recorded of the deuterated compounds $[Ln(OS(CD_3)_2)_8]I_3$ and $[Y(OS(CD_3)_2)_8]I_3$ (experimental frequencies are listed in Table S3) to ascertain the assignment of the bands and to increase the number of available normal modes for evaluating force constants in the normal coordinate analyses. In the CH_3 and CD_3 stretching regions with six fundamental modes, ν_1, ν_2, ν_3, ν_{14}, ν_{15}, and ν_{16}, five well-defined bands were observed. The symmetric CD_3 stretching bands (ν_1, ν_2) at 2120 cm^{-1} were the strongest Raman features in this region. Three bands in the ranges 1405−1442 and 1006−1031 cm^{-1}, were ascribed to the four asymmetric deformation modes of the CH_3 and CD_3 groups, respectively.

For the symmetric deformations, the umbrella modes of the methyl groups, three IR ($B_2 + 2E_1$) and five Raman ($A_1 + 2E_2 + 2E_3$) frequencies are expected within the D_{4d} point group symmetry. The umbrella modes were observed in the ranges 1292−1356 for CH_3 and 999−1061 cm^{-1} for CD_3, which indicates weak vibrational coupling between the symmetric deformations of the methyl groups. The experimental observations displayed all three IR modes, but only three of five Raman features were observed in the spectral region of CH_3/CD_3 symmetric deformations. The assignment becomes difficult without the "missing" bands and relies on a normal coordinate calculation for the full complex. For the previously investigated six-coordinated $[Sc(OS(CH_3)_2)_6]^{3+}$ complex, we observed only two corresponding bands with a separation of about 20 cm^{-1},[19] indicating that vibrational coupling via the central metal atom is almost absent. The methyl rocking modes showed similar behavior as the asymmetric deformation vibrations. Generally, two in-phase (ν_7, ν_8) and two out-of-phase (ν_{20}, ν_{21}) modes were observed for the complexes, both for $(CH_3)_2SO$ and $(CD_3)_2SO$ as ligands. Characteristic methyl group vibrations occurring above 1000 cm^{-1} are summarized in Table S5.

For the $[Ln(OS(CH_3)_2)_8]^{3+}$ complexes with Ln = Y, La, Ce, Pr, Nd, Gd, Tb, Dy, Er, and Lu, assignments of the fundamental skeletal modes, which are observed below 1000 cm^{-1}, are presented in Table 4. The new bands observed in the region 400−450 cm^{-1} can be assigned as Ln−O stretching modes (Figure 3). The two IR-active bands could be assigned as the B_2 (with higher intensity) and E_1 symmetry species. The relative intensities of the Raman bands support the assignment of the stronger low-frequency bands to the symmetric A_1 stretching mode and the weaker high-frequency bands to the E_2 and E_3 modes of the Ln−O stretching vibrations. The increase of the averaged Ln−O stretching frequency from 408 ($[La(OS(CH_3)_2)_8]^{3+}$) to 432 cm^{-1} ([Lu-

Table 4. Assignment of IR and Raman Fundamental Modes (cm^{-1}) of Octakis(DMSO)lanthanoid(III) Complexes

$Y(OSMe_2)_8I_3$			$La(OSMe_2)_8I_3$			$Ce(OSMe_2)_8I_3$			$Pr(OSMe_2)_8I_3$			$Nd(OSMe_2)_8I_3$					
IR	Raman	calcd	IR	Raman	calcd	IR	Raman	calcd	IR	Raman	calcd	IR	Raman	calcd	PED, %	assignment	
970(60)[a]	967 sh[b]	973	968(65)		973	962(100)		962	963(100)		963	964(100)	966 sh	964	89ν(SO)	B_2	$\nu_9(A')$[c], ν(SO)[d]
960 sh	961(9)	965	960 sh	966(11)	970		963(13)	963		959(15)	959		958(4.8)	958	8ν(MO)	A_1	
941 sh	941 sh	943	946 sh	947 (4)	954	946(36)		946	956(64)		956	943(46)		943		E_1	
	908(2)	906		915(2)	922		947(3)	947	942 sh	946 sh	946		948(3)	948		E_2	
912(19)		916	918(7)		914		937sh	937		935 sh	935		925(1)	925		E_3	
						907 (4)				916 vw							
	714(35)	714		713(22)	711		716(39)	716		715(35)	715		714(34)	714	98 $\nu_a(SC_2)$	E_2, E_3	$\nu_{22}(A'')$, $\nu_a(SC_2)$
713(24)		713	712(11)			714 (19)		715	715(16)		715	718(18)		718		E_1	
	682(100)	683		676(66)	679		678(100)	678		679(100)	679		679(100)	679	95 $\nu_s(SC_2)$	A_1, E_2, E_3	$\nu_{10}(A')$, $\nu_s(SC_2)$
678(11)		684	676(2)		679	678(3)		678	678(6)		678	682 vw		682		B_2	
678(11)		684	676(2)		679	668(1)		668	667(6)		667	643 vw		643		E_1	
424(8)		419	408(4)		404	411(21)		411	411(26)		411	409 (37)		409	70ν(MO), 17$\omega(SC_2)$	B_2	ν(LnO)[e]
	415(7)	412		402(5)	396		403(8)	403		410(9)	410		409(7)	409	55 ν(MO), 32 $\omega(SC_2)$	A_1	
	415(7)	409		410 sh	402		426(1)	426		419(4)	419		428 sh	428	50 ν(MO), 40 $\omega(SC_2)$	E_2, E_3	
416 sh		411	408(4)		400	403(18)		403	407(24)		407	413 sh		413	71 ν(MO), 13 $\omega(SC_2)$	E_1	
382(2)	396 sh			391 sh		389 (10)	393(2)		384(12)	388 sh		386(13)	385 vw				2 ω (SC_2)
	355(13)	359		358 sh	355		350 sh	350		351 sh	351		353 sh	353	94 $\delta(SC_2)$	E_2, E_3	$\nu_{11}(A')$, δ (SC_2)
350(6)		356	348(3)		360	346(13)		346	350(26)		350	347(36)		347		B_2	
	344(26)	348		345(10)	351		347(16)	347		344(21)	344		350(35)	350		A_1	
360 sh		363	360 sh			350		332	334(20)		334	337(24)		337		E_1	
318(8)		312	314(13)		308	316(8)		316	315(12)		315	315(15)		315	98 $\tau(SC_2)$	E_1	$\nu_{23}(A'')$, τ (SC_2)
	315(29)	305		313(16)	306		314(24)	314		313(31)	313		313(35)	313		E_2, E_3	
219(6)		221	186(32)		186	188(18)		188	189(22)		189	193(24)		193	75 $\omega(SC_2)$, 8 ν(MO)	E_1	$\nu_{12}(A')$, ω (SC_2)
191 sh	197(1)	196		190(3)	187		188(1)	188		189(4)	189		193 vw	193	68 $\omega(SC_2)$, 15 ν(MO)	A_1	
219(6)		221	186(32)		186	188(18)		188	189(22)		189	189(31)		189	61 $\omega(SC_2)$, 17 ν(MO)	B_2	
							183(1)	183		175(3)	175		189 vw	189	58 $\omega(SC_2)$, 28 ν(MO)	E_2, E_3	
									276 vw	267 vw							OMO skeletal deformations, methyl torsional, and DMSO skeletal torsional modes
										236 vw		248 sh					
									210 sh			212(16)					
						154(34)			158 sh			154(19)					
										144(6)							
										114 vw							
									99 vw			107 vw					
									66 vw			89(8)					

Table 4 (Continued)

$Gd(OSMe_2)_8I_3$			$Tb(OSMe_2)_8I_3$			$Dy(OSMe_2)_8I_3$			$Er(OSMe_2)_8I_3$			$Lu(OSMe_2)_8I_3$					
IR	Raman	calcd	IR	Raman	calcd	IR	Raman	calcd	IR	Raman	calcd	IR	Raman	calcd	PED, %	assignment	
962(100)		962	966(100)		966	967(100)		967	968(100)		968	962(100)		962	89ν(SO), 8ν(MO)	B_2	ν_9(A′), ν(SO)
	963(12)	963		964(10)	964		965(4)	965		964(12)	964		963(10)	963		A_1	
939(94)		939	943(49)		943	938(94)		938	942(58)		942	939(94)		939		E_1	
	943(5)	945		940(6)	940		950(2)	950		944(5)	944		947(5)	947		E_2	
	941(3)	941		918(2)	918		936 (1)	936		941(4)	941		941(5)	941		E_3	
	912(1)		926 sh			904(70)	914 vw		906(11)	912(1)			908(1)				
	715(43)	715		714(48)	714		721(23)	721		715(43)	714		715(43)	715	98 $\nu_a(SC_2)$	E_2, E_3	ν_{22}(A″), $\nu_a(SC_2)$
714(29)		714	717(70)		717	715(16)		715	714(22)		718	712(40)		712		E_1	
	684(100)	684		680(100)	680		681(100)	681		684(100)	679		684(100)	684	95 $\nu_s(SC_2)$	A_1, E_2, E_3	ν_{10}(A′), $\nu_s(SC_2)$
677(15)		677	679(7)		679	679(49)		679	684(11)		682	682(6)		682		B_2	
640 sh		641	679(7)		679	641(48)		641			643	674(5)		674		E_1	
414(53)		418	418(20)		418	420(43)		420	422(31)		422	423(29)		423	70ν(MO), 17 $\omega(SC_2)$	B_2	ν(LnO)
	417(5)	417		414(5)	414		410(9)	410		419(8)	419		417(5)	417	55 ν(MO), 32 $\omega(SC_2)$	A_1	
	431(1)	432		433(2)	433		429(4)	429		438(1)	438		432(1)	432	50 ν(MO), 40 $\omega(SC_2)$	E_2, E_3	
418(38)		418	418(20)		418	435(14)		435	436(21)		436	443(20)		443	71 ν(MO), 13 $\omega(SC_2)$	E_1	
384(15)	395 (1)			398(2)			388 sh		386(13)	385 vw		386(15)	395 (1)				2 ω (SC_2)
	355(12)			350(11)	350		351 sh	351		357(13)	357		355(12)	355	94 $\delta(SC_2)$	E_2, E_3	ν_{11}(A′), δ (SC_2)
351(49)		351	349(23)		349	353(17)		353	350(31)		350	353(43)		353		B_2	
	345(16)	345		342(13)	342		344(21)	344		346(15)	346		345(16)	345		A_1	
347(54)		347	349(23)		349	338(18)		338	338(22)		338	341(32)		341		E_1	
316(24)		316	318(13)		318	316(17)		316	318(10)		318	317(28)		317	98 $\tau(SC_2)$	E_1	ν_{23}(A″), $\tau(SC_2)$
	316(28)	316		312(19)	312		313(31)	313		317(30)	317		316(28)	316		E_2, E_3	
			282(10)														
			204(15)														
195 sh		195	195(17)		195	201(37)		201	186(22)		193	195(46)		195	75 $\omega(SC_2)$, 8 ν(MO)	E_1	ν_{12}(A′), $\omega(SC_2)$
	191(7)	191		170(1)	169		189(4)	189		202(6)	193		191(7)	191	68 $\omega(SC_2)$, 15 ν(MO)	A_1	
187(51)		187	189(27)		187	171(49)		171	177(25)		189	172(66)		172	61 $\omega(SC_2)$, 17 ν(MO)	B_2	
	166(4)	168		165 vw	165		175(3)	175		173(2)	189		166(4)	168	58 $\omega(SC_2)$, 28 ν(MO)	E_2, E_3	
			174(25) sh														
172 (43)			130(6) sh							160(1)		152(33)	156(6)				OLnMO skeletal deformations, methyl torsional and DMSO skeletal torsional modes
140 (19)						147(22)	144(3)										
						137(20)	138 vw			140(0.1)			139(7)				
106 vw						100(9)			104(7)			100(10)	99(0,1)				
89(4)																	

[a] Numbers in brackets are relative intensities of the bands on a scale from 0 to 100. [b] sh denotes shoulders near the strong bands; their positions have been determined using second derivatives of the spectra. [c] The DMSO and DMSO-d_6 normal mode numbering refers to the notation of the fundamentals for the free DMSO molecule.[19] The *A′* and *A″* species reflect the plane of symmetry of the DMSO molecule (in the C_s point group). [d] The normal vibrations ν_a (ν_a'), δ_a (δ_a'), and ρ (ρ') denote the stretching, bending, and rocking pairs of CH_3/CD_3 modes, respectively, with dipole changes in (or perpendicular to) the plane of symmetry; ν_s, symmetric CH_3/CD_3 stretch; δ_s, symmetric deformation (umbrella mode), ω, wagging, and τ, twisting modes. [e] Assignment of skeletal modes of the complex in the D_{4d} point group. [f] Band intensities: vs = very strong; vw = very weak; vvw = very, very weak; sh = shoulder.

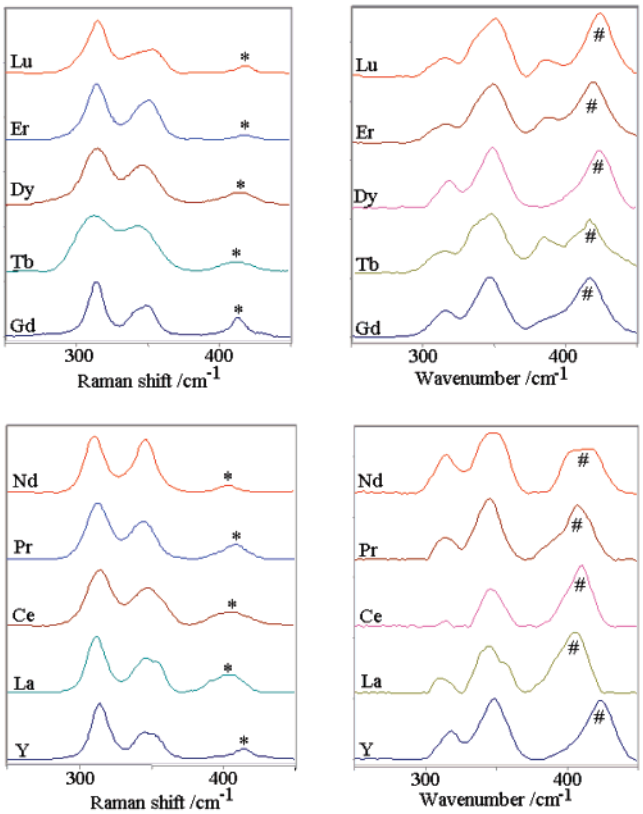

Figure 3. Raman (left) and IR absorption (right) spectra of the $[Ln(OSMe_2)_8]I_3$ compounds in the region 250−450 cm^{-1}. The symbol * indicates totally symmetric (A_1) Ln−O stretching frequencies, and the symbol # indicates the asymmetric (B_2) Ln−O stretching frequencies.

$(OSMe_2)_8]^{3+}$) reflects the increase in bond strength due to the lanthanoid contraction. In such qualitative correlations, the use of the averaged frequency, $\bar{\nu} = (\nu_{A1} + \nu_{B2} + 2\nu_{E1} + 2\nu_{E2} + 2\nu_{E3})/8$ for the eight Ln−O stretchings is recommended, instead of merely introducing the frequency of the symmetric stretching A_1 mode because the effects of ligand−ligand interactions to some extent cancel in the average.[33]

In the S−O stretching region, 3−4 Raman bands of medium to low intensity were observed for the series of lanthanoid(III) solvates. The stronger high-frequency band (958−966 cm^{-1}) was assigned as the A_1 symmetry species and the low-frequency shoulders as the E_2 and E_3 vibrational modes. The strongest band in the IR spectra is a well-defined doublet, at 962−970 cm^{-1} with a shoulder at 939−956 cm^{-1}, which can be ascribed to the B_2 and E_1 symmetry species, respectively. Deuteration does not significantly shift these bands, which supports their assignment as S−O stretchings. The presence of some additional bands in this spectral region could be explained by the deviation from D_{4d} point group symmetry, allowing forbidden modes to appear and degenerate modes to split, or by the appearance of overtones and combination bands.

Two sets of bands around 700 cm^{-1} were attributed to the SC_2 asymmetric (712−721 cm^{-1}) and symmetric (lower than 700 cm^{-1}) stretching modes; the latter constitute the most intense Raman bands in the spectra. For the asymmetric and symmetric SC_2 stretching modes, deuteration induces the most significant downshifts of ligand skeletal modes observed in the spectra, 73 and 55 cm^{-1}, respectively. All skeletal deformation modes of DMSO (ν_{11}, ν_{12}, and ν_{23}) downshifted at coordination but with less pronounced shifts than for the above C−S stretching modes.

Well-defined intense IR absorption bands at 330−360 cm^{-1} can be assigned as SC_2 scissoring (ν_{11}) modes belonging to the B_2 (more intense) and E_1 symmetry species, respectively. The strong Raman band near 345 cm^{-1} can be assigned as an A_1 mode, and the shoulder at higher frequency (ca. 350 cm^{-1}) to modes of E_2 and E_3 symmetry.

The SC_2 twisting mode (ν_{23}) was ascribed to a strong Raman band at 312−317 cm^{-1} (at 271 cm^{-1} in the deuterated samples). In the IR spectra, this mode is observed as a medium-intensity band at 314−318 cm^{-1} (281 and 277 cm^{-1} for $[Y(OS(CD_3)_2)_8]^{3+}$ and $[La(OS(CD_3)_2)_8]^{3+}$, respectively). The SC_2 wagging (ν_{12}) is assigned to the weak-to-medium-intensity band at 170−201 cm^{-1}. Other low-frequency vibrational frequencies observed in experimental spectra can tentatively be attributed to LnOS deformation, deformations of LnO_8 polyhedra, methyl group torsions, and C_2SO skeletal torsional modes (Table 4).

An additional low-intensity vibrational mode is observed in almost all spectra in the region 380−390 cm^{-1}. The assignment of this band is not obvious: the frequency is rather high for SC_2 scissoring and somewhat too low for Ln−O stretching. The fairly small shifts of this band for different central atoms suggest that this band could arise from the first overtone of the SC_2 scissoring mode enhanced by interaction with the close Ln−O stretching frequency. The relative intensities of these bands also support this assignment.

Discussion

Oxygen-coordinated DMSO ligands in crystalline solvates of high-valent metal ions frequently show partial disorder, often by an inverted configuration of the pyramidal molecule, allowing only the alternative sulfur position to be resolved. However, even such a 180° twist around the Ln−O bond direction will affect the oxygen atom position. A description of the unresolved displacement of the oxygen atom for such a disordered ligand by means of an enlarged thermal ellipsoid will result in a too-short Ln−O bond distance.[5,34] The disorder in the present $[Ln(OS(CH_3)_2)_8]^{3+}$ complexes corresponds, however, to smaller twists around the Ln−O bond, and the refinements could be performed assuming semirigid complete DMSO molecules in two alternative sites, see Crystallography. This approach seems to yield reliable Ln−O bond distances at least for the main site, and the weighted mean La−O bond distance of **1**, 2.490 Å, is close to that reported for the eight-coordinated complex in the $[La(OS(CH_3)_2)_8][(\mu\text{-}WSe_4)_3Ag_3]$ compound, 2.492 Å.[7] An EXAFS study of solid $[La(OS(CH_3)_2)_8]I_3$ gave a mean La−O bond distance of 2.495 Å; EXAFS is lattice independent, and alternative orientations of the DMSO ligands will not

(33) Mink, J.; Nemeth, Cs.; Hajba, L.; Sandström, M.; Goggin, P. L. *J. Mol. Struct.* **2003**, *661−662*, 141−151.

(34) Sandström, M. *Acta Chem. Scand. A* **1978**, *32*, 519−525.

Table 5. Refined Force Constants for $[Ln(OS(CH_3)_2)_8]I_3$ Compounds[a,b]

coordinate	DMSO (OSC_2)	Y	La (**1**)	Ce (**2**)	Pr (**3**)	Nd (**4**)	Gd (**5**)	Tb (**6**)	Dy (**7**)	Er (**8**)	Lu (**9**)
					Stretch						
K(MO)	−	1.490	1.432	1.445	1.456	1.462	1.478	1.483	1.489	1.493	1.496
K(SO)	5.060	4.677	4.545	4.573	4.601	4.627	4.657	4.664	4.663	4.683	4.691
K(CS)	2.060	2.244	2.251	2.249	2.247	2.265	2.241	2.252	2.246	2.259	2.228
					Stretch−Stretch						
F(CS, CS)	0.230	−0.014	−0.014	−0.023	−0.037	−0.042	−0.027	−0.038	−0.035	−0.026	−0.021
					Bend						
H(SC_2)	1.141	0.961	0.976	0.926	0.895	0.919	0.930	0.919	0.905	0.921	0.918
H(CSO)	0.947	0.630	0.618	0.621	0.623	0.611	0.633	0.620	0.612	0.624	0.627
					Bend−Bend						
K(CSO, CSO)	0.052	−0.031	−0.035	−0.036	−0.037	−0.032	−0.036	−0.027	−0.024	−0.038	−0.032
					Stretch−Bend						
H(MO, SC_2)	−	0.086	0.072	0.066	0.076	0.081	0.068	0.075	0.078	0.079	0.067

[a] Force constant units: stretching (*K*, *F*) in 10^{-2} N·m^{-1}, stretching−bending (*k*) and bending−bending (*h*) in 10^{-6} N·rad^{-1}, and bending (*H*) in 10^{-16} Nm·rad^{-2}. [b] Methyl groups treated as point masses.

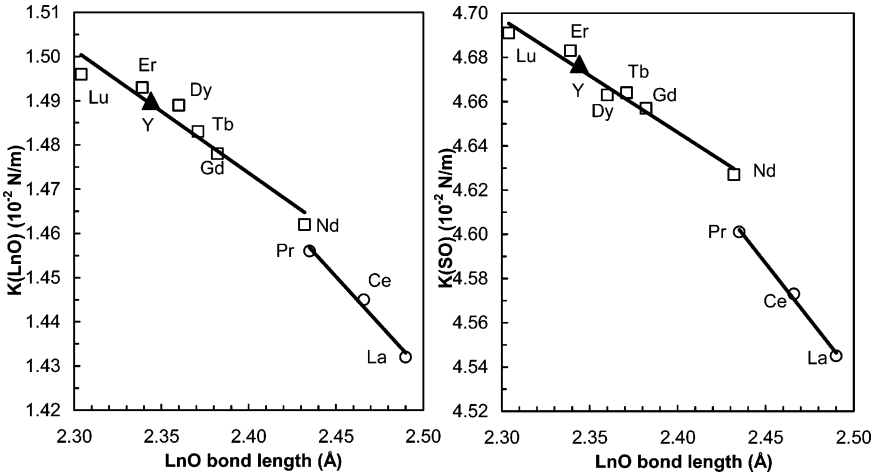

Figure 4. Force constants for (left) Ln−O and (right) S−O stretching vibrations vs mean Ln−O bond lengths for the DMSO solvates $[Ln(OS(CH_3)_2)_8]I_3$.

affect the La−O bond distances.[35] Also, the mean Gd−O bond distance of 2.393 Å in octakis(DMSO)gadolinium(III) hexacyanoferrate(III) is close to that in **6**, 2.382 Å.[12] The mean Pr−O bond distance, 2.454 Å, in the $[Pr(OS(CH_3)_2)_8]_2(PMo_{10}V_2O_{40})(NO_3)\cdot(CH_3)_2SO$ compound with discrete $[Pr(OS(CH_3)_2)_8]^{3+}$ complexes,[10] is slightly longer than that for **3**, 2.435 Å, while for the coordination number 9 in the polymeric structure of $[\{Pr(OSMe_2)_6(H_2O)\}(PMo_{12}O_{40})\cdot CH_3CN]_n$, the reported value is similar, 2.429 Å.[36]

The S−O bond has partial double bond character, and a recently published comprehensive review concerning the structure and bonding in coordinated sulfoxide compounds[4] confirmed that the S−O bond distance becomes shorter in S-coordinated sulfoxide complexes, the reported mean value is 1.4738(7) Å, with respect to that of uncoordinated sulfoxides, 1.492(1) Å. The opposite occurs for O-bonded ligands, for which the mean S−O bond distance, 1.528(1) Å, can be compared with the values obtained for the ordered DMSO ligands of the current compounds, Table 3. Those values vary around 1.50 Å, while the *K*(SO) stretching force constants (Table 5) only increase slightly from 4.55 (La) to 4.69 N·cm^{-1} (Lu), justifying the semirigid model introduced for the disordered ligands. The coordination bond to the oxygen atom reduces the π-electron transfer from oxygen to sulfur, corresponding to the concurrent increase in the Ln−O stretching force constant (Figure 4), and explains the increase in the S−O bond length with respect to uncoordinated DMSO.[4,5] When the lanthanoid(III) ions contract along the lanthanoid series from lanthanum to lutetium, their decreasing size enhances the Ln-O bond strength. The charge difference between the O and S atoms increases and induces a σ-electron transfer from the sulfur to the oxygen atom resulting in the fairly constant average S−O bond distances in the studied complexes.

Even though the electron configuration of the outer valence shell of the lanthanoid(III) ions remains similar, the mean LnOS angle decreases, from 138.3° for La to 131.4° for Lu, in the series of octakis(DMSO)lanthanoid(III) iodides (Figure 2). An increase in covalency for the smaller Ln(III) ions would require a smaller LnOS angle to maximize the orbital overlap and increase the bond strength.[25] The increasing tendency striving to decrease the LnOS angle could be the driving force for the transition from the more efficient packing in the orthorhombic lattice with closer anion−cation

(35) Persson, I.; Damian Risberg, E.; D'Angelo, P.; De Panfilis, S.; Sandström, M.; Abbasi, A. *Inorg. Chem.* **2007**, *46*, 7742−7748.
(36) Niu, J.- Y.; Wei, M.-L.; Wang, J.- P. *J. Mol. Struct.* **2004**, *689*, 147−152.

distances to the monoclinic structures (Figure 2). An increasing number of DMSO ligands with alternative positions seems to be related to the increase in volume for those smaller lanthanoid(III) ions, cf. Table 3.

In the vibrational spectra, the greatest changes with decreasing size of the central lanthanoid(III) ion occur, as expected, for the Ln−O stretching frequencies. Almost linear correlations between the Ln−O and S−O stretching force constants and the Ln−O bond lengths are found in Figure 4, with a distinct break at the change in space group symmetry between Pr and Nd. Qualitative correlations have been reported between the S−O bond distance for sulfoxides and the strongest S−O stretching frequency, ν(SO), in the IR spectra (in our notation $\nu_9(A')$ of the B_2 symmetry species).[4,5] Table 4 shows that the frequencies of the Ln−O stretching smoothly increase with decreasing Ln−O distances. However, the frequency changes are affected by coupling between the Ln−O stretching and some SC_2 wagging modes, depending on their symmetry species (see below). Hence, it is more satisfactory to correlate force constants, instead of frequencies of certain modes, with the properties of the bonds.

Even though the lanthanoid(III) series is favorable for discussing trends, one should keep in mind that bond strength comparisons are based on the assumptions that the shape of the potential well of the metal−ligand bond and the effects of ligand−ligand repulsion are similar. The force constant is a measure of the curvature of the potential surface near the equilibrium position of the bond distance, while the depth of the potential energy curve measures the dissociation energy of the bond.[37] The larger the force constant, the sharper the curvature near the bottom of the potential well, but that does not necessarily correspond to a deeper potential well.

Ln−O stretching force constants vs Ln−O bond lengths are compared in Figure 5 for the present DMSO solvates with the octahedral hexakis(DMSO) complexes of Sc and of Group 13 metal ions[19,25] and also with the force constants of the tricapped trigonal prisms of nonahydrated lanthanoid(III) ions in trifluoromethanesulfonate salts from our previous work.[38] The mean Ln−O(DMSO) bond distances decrease by 7% from La to Lu (Table 3), while the stretching force constants increase by 4% (Table 5). The corresponding changes for the force constants of the nonahydrated lanthanoid(III) ions are significantly larger.[38] In the trigonal LnO_6 prism of the hydrates, the decrease in bond length from La to Lu is 9% (from 2.52 to 2.29 Å), while the corresponding increase in Ln−O stretching force constants is 30% (from 0.807 to 1.158 N·cm^{-1}). Similar effects were found for the capping Ln−O bonds, for which bond shortening by 4% (from 2.61 to 2.51 Å) leads to a 25% increase in the force constants (from 0.488 to 0.650 N·cm^{-1}), even though the correlation deviates for the smallest ions lutetium(III) and ytterbium(III), because of the increased ligand−ligand repulsion and significant water deficit.[38,39]

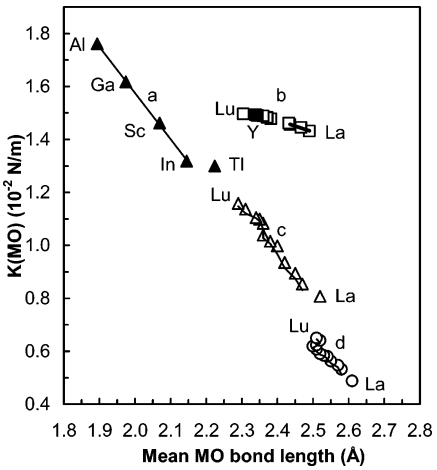

Figure 5. M−O force constants vs M−O bond distances for (a) $[M(OSMe_2)_6]^{3+}$ complexes, M = Al, Ga, In, Tl, and Sc (▲); (b) $[Ln(OS(CH_3)_2)_8]^{3+}$, Ln = La, Ce, Pr, Nd, Gd, Tb, Dy, Er, Lu (□), and Y(■); (c) $[Ln(H_2O)_9]^{3+}$ complexes, Ln = La, Pr, Nd, Sm, Gd, Tb, Dy, Ho, Er, Tm, Yb, and Lu for trigonal prism (Δ); and (d) capping (○) Ln−O distances.

The force constants are much higher for similar Ln−O bond lengths in DMSO solvates than in hydrates of the lanthanoid(III) ions (cf. Figure 5). The stronger coordination of DMSO is also evident in mixed-ligand complexes with water and DMSO. For the discrete $[Ce(OSMe_2)_6(H_2O)_2]^{3+}$ complex, the mean Ce−O bond distance is 2.447 Å for the six DMSO ligands in a well-determined crystal structure (2.465 Å for the fully octasolvated cerium(III) ion), while the Ce−O bond distance to the two aqua ligands is 2.517(2) Å.[40] The previously determined $[Y(OSMe_2)_2(H_2O)_6]Cl_3$ structure[41] was re-evaluated with the same type of restrained model with alternative positions for both disordered DMSO ligands. This resulted in a mean Y−O(dmso) distance of 2.272 Å, which is much shorter than the mean Y−O value 2.344 Å for the fully octasolvated complex, Table 3, while the average Y−O distance to the six water molecules is 2.38 Å.

The sensitivity of the bond distance to the coordination is evident, e.g., for the nitrates, where a slightly shorter average La−O distance, 2.470 Å, is reported for the coordinated DMSO ligands of the $[La(OS(CH_3)_2)_4(NO_3)_3]$ complex, where the nitrate groups act as bidentate ligands increasing the coordination number to 10.[18] Also for the $[Lu(OS(CH_3)_2)_3(NO_3)_3]$ compound, again with bidentate nitrate ligands, the mean Lu−O(DMSO) bond distance 2.228 Å is considerably shorter than for **9**, 2.303 Å.[18] The short Ln−O(DMSO) distances in the solvated lanthanoid(III) nitrates indicate weakly bonded nitrate groups.

The force constants, K(MO), for the octahedral hexacoordinated DMSO solvates of the Group 13 trivalent ions[25]

(37) Nakamoto, K. *Infrared and Raman Spectra of Inorganic and Coordination Compounds*, 5th ed.; John Wiley and Sons: New York, 1997.
(38) Mink, J.; Skripkin, M. Yu.; Hajba, L.; Németh, C.; Abbasi, A.; Sandström, M. *Spectrochim. Acta A* **2005**, *61*, 1639−1645.
(39) Abbasi, A.; Lindqvist-Reis, P.; Eriksson, L.; Sandström, D.; Lidin, S.; Persson, I.; Sandström, M. *Chem. Eur. J.* **2005**, *11*, 4065−4077.
(40) Chen, L.-J.; Lu, C.-Z.; Zhang, Q.-Z.; Chen, S.-M. *Acta Crystallogr.* **2005**, *C61*, m269−m271.
(41) Kristiansson, O.; Lindqvist-Reis, P. *Acta Crystallogr.* **2000**, *C56*, 163−164.

also increase significantly, 25% (from 1.318 to 1.761 $N \cdot cm^{-1}$) when decreasing the M−O bond distances 12% from 2.145 to 1.894 Å for indium(III) to aluminum(III), respectively. The $[Sc(OS(CD_3)_2)_6]^{3+}$ complex of the Group 3, with the Sc−O distance 2.069 Å and the stretching force constant 1.462 $N \cdot cm^{-1}$,[19] follows the correlation for the hexacoordinated Group 13 ions. The $[Tl(OS(CH_3)_2)_6]^{3+}$ complex deviates with an Tl−O bond length of 2.224(3) Å, a TlOS angle of 120.7(2)°,[42] and a stretching force constant of 1.300 $N \cdot cm^{-1}$. Its S−O stretching force constant, 4.279 $N \cdot cm^{-1}$, is smaller than that for the isostructural scandium(III) compound, 4.402 $N \cdot cm^{-1}$,[19] and also lower than the values obtained for the octakis(DMSO)lantanide(III) solvates (Table 5), an effect of the higher covalency in the Tl^{III}−O bonds.[25]

The changes in the Ln−O stretching force constants in the series of DMSO solvates are much smaller than for the hydrated ions, probably because of the stronger steric interactions between the more space-demanding DMSO ligands (Figure 5). For the S−O and the C−S stretching modes, the force constants vary only 3.1% and 1.0%, respectively (cf. Table 5), in the lanthanoid(III) series.

The deformation modes for the coordinated DMSO ligands decrease, in comparison with DMSO molecules in the neat liquid,[19] due to the interaction with the MO stretching mode. For the SC_2 twisting (ν_{23}), no coupling with the MO stretching is observed and the frequency decrease is small (ca. 15 cm^{-1}). All other modes in that spectral region are more strongly coupled with the Ln−O stretching, e.g., the SC_2 scissoring (ν_{11}) frequency decreases ca. 40 cm^{-1} with weak metal ion dependence. The SC_2 wagging mode (ν_{12}) shows the largest shift with up to 100 cm^{-1}, especially for the heavy metal ions (Table 4). Thus, the most significant coupling occurs for the E_2 and E_3 modes and is far less for the B_2 and E_1 normal modes, which is also expected from the corresponding atomic displacements.

Conclusions

The crystal structures of the solvated lanthanoid(III) iodides, $[Ln(OS(CH_3)_2)_8]I_3$, comprise discrete octakis(DMSO)lanthanoid(III) complexes and iodide ions. As expected from the general decrease in ionic radii from light to heavy rare earth ions, the mean Ln−O bond distances decrease from 2.49 to 2.30 Å along the series of lanthanoid(III) ions. The increasing S−O and Ln−O force constants and the concurrent decrease in the mean LnOS bond angles indicate that the increasing polarization of the Ln−O bonds probably is the cause of the change in unit cell symmetry. The solvates of the largest ions, Ln = La, Ce, and Pr, crystallize in the orthorhombic space group *Pbca*, while the smaller ions, Ln = Nd, Sm, Gd, Er, Lu, and also Y, were characterized in the monoclinic space group $P2_1/n$. The less-efficient packing of the $[Ln(OS(CH_3)_2)_8]^{3+}$ complexes and the iodide ions in the monoclinic unit cell for the smaller lanthanoid(III) ions (Figure 2) seems related to an increase in positional disorder of the DMSO ligands.

Complete assignments of the vibrational frequencies for all skeletal normal modes of the octakis(DMSO)lanthanoid(III) complexes have been achieved. Several vibrational frequencies of the coordinated DMSO ligands showed substantial changes. Force constants obtained by normal coordinate analyses for both the Ln−O and S−O stretching modes showed significant increases related to the decreasing ionic size in the lanthanoid series. That increase was, however, hampered by strong ligand−ligand interactions for the smallest lanthanoid(III) ions.

Acknowledgment. We gratefully acknowledge the Swedish Research Council and the Hungarian National Research Foundation (OTKA T025278 and TO35115) for financial support. The Swedish and Hungarian Academies of Science are acknowledged for the support of our cooperation and the Swedish Institute for support through the Visby programme. We thank Dr. Eva Bencze for assistance with the vibrational spectroscopic experiments.

Supporting Information Available: Description of internal and symmetry coordinates, averaged skeletal and characteristic methyl group modes for $[Ln(OSMe_2)_8]^{3+}$ (Ln = Y, La, Ce, Pr, Nd, Gd, Tb, Dy, Er, Lu) complexes, and crystallographic data. This material is available free of charge via the Internet at http://pubs.acs.org.

IC7006588

(42) Ma, G.; Molla-Abbassi, A.; Kritikos, M.; Ilyukhin, A.; Jalilehvand, F.; Kessler, V.; Skripkin, M. Yu.; Sandström, M.; Glaser, J.; Näslund, J.; Persson, I. *Inorg. Chem.* **2001**, *40*, 6432−6438.